Eur. Phys. J. Spec. Top.
https://doi.org/10.1140/epjs/s11734-025-01649-1

THE EUROPEAN PHYSICAL JOURNAL SPECIAL TOPICS

Regular Article

In-line monitoring of a multi-stage drying process for battery electrodes: vol. 2—advancing measurement techniques with chromatic confocal sensors

Jonas Mohacsi[1,2,a], Kevin Ly[1,2,b], Jannes Hohlweck[1], Philip Scharfer[1,2,c], and Wilhelm Schabel[1,2,d]

[1] Thin Film Technology, Karlsruhe Institute of Technology, Kaiserstraße 12, 76131 Karlsruhe, Germany
[2] Material Research Center for Energy Systems (MZE), Karlsruhe Institute of Technology, Kaiserstraße 12, 76131 Karlsruhe, Germany

Received 7 January 2025 / Accepted 24 April 2025

Abstract The drying of electrode coatings represents a critical stage in the battery production process, where even slight deviations in drying conditions can lead to defects, resulting in high rejection rates, increased costs, and material waste. To address these challenges, the integration of in-line measurement technologies offers a promising solution. Following the investigation of scattered light sensors in vol. 1 of the study Mohacsi et al. (in Eur Phys J Special Topics, 1–9, 2024), the present work explores the potential of chromatic confocal sensors for monitoring the drying process of electrodes. A dual-sided measurement system employing two chromatic confocal point sensors was established, enabling precise layer thickness measurements even on a substrate belt significantly affected by vibrations. It was demonstrated that the standard deviation of the thickness signal serves as a reliable metric for characterizing surface roughness. Initial drying experiments compared the signal profiles of the chromatic confocal sensors with those of the previously studied scattered light sensor. This comparison provided strong evidence that chromatic confocal sensors can reliably detect key points during drying, such as the onset of pore-emptying. In further experiments, the layer thickness measurements from the confocal sensors were combined with gravimetric determinations of layer porosity, offering deeper insights into the mechanisms occurring during drying. Overall, the results suggest that chromatic confocal sensors could be a valuable tool not only for quality assurance during drying but also for optimizing the configuration of a three-stage drying process.

1 Introduction

The demand for lithium-ion batteries (LIBs) continues to grow rapidly, driven by the global transition to renewable energy systems and the expansion of electric mobility. [1] This growth places increasing pressure on battery manufacturers to enhance production efficiency while maintaining high product quality. A critical step in the production process is the drying of battery electrodes, where even minor inconsistencies can lead to defects that compromise battery performance, safety, and lifespan. These defects often result in high rejection rates, increasing production costs and material waste. [2] To address these challenges, the integration of in-line measurement technologies offers a promising solution. These technologies enable real-time monitoring and control of the drying process, allowing for early detection and correction of inconsistencies.

In vol. 1 of this publication "In-line monitoring of a multi-stage drying process for battery electrodes: Vol. 1 - Applying methods of scattered light measurement" [3], the use of a scattered light sensor to detect key characteristic time points during the drying process was investigated. This approach proved to be beneficial for implementing and monitoring a three-stage drying process. Building on this foundation, the present study explores the use of chromatic confocal sensors for monitoring the drying progress. While chromatic confocal sensors are an

[a] e-mail: jonas.mohacsi@kit.edu (corresponding author)
[b] e-mail: kevin.ly@kit.edu
[c] e-mail: philip.scharfer@kit.edu
[d] e-mail: wilhelm.schabel@kit.edu

Published online: 13 May 2025

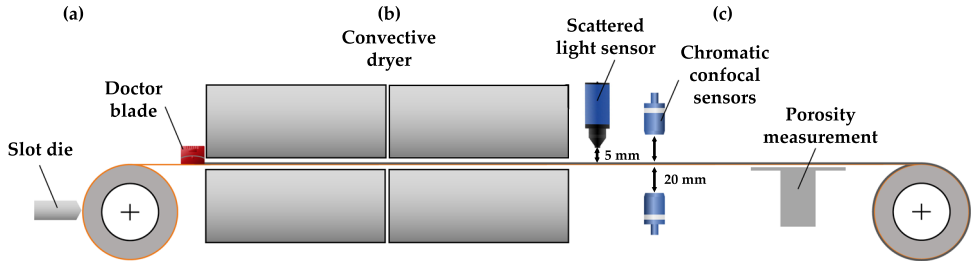

Fig. 1 Setup for drying experiments: **a** coating zone allowing for slot-die or doctor blade coating; **b** convective dryer with two zones; **c** measurement section including dual-sided chromatic confocal sensors, a scattered light sensor and the porosity measurement

established tool for in-line layer thickness measurement, this study aims to leverage their signals to characterize electrode surfaces during drying. Similar to the investigation using the scattered light sensor, this approach seeks to identify critical milestones in the drying process. The fundamental principles of microstructure formation during drying, including processes such as pore-emptying and binder migration, as well as the conceptual framework for a multi-stage drying process, were comprehensively detailed in vol. 1 of the study. Readers seeking a deeper understanding of these foundational topics are encouraged to consult vol. 1 or the original sources cited therein. [3–9]

2 Experimental setup

2.1 Coating and drying setup

Figure 1 illustrates the applied setup for the drying experiments consisting of a laboratory-scale roll-to-roll system (Coatema Basecoater). Coating is performed via either conventional slot-die coating or doctor blade coating. Due to the lower complexity of the process and the relatively high tolerance for coating defects, all experiments conducted in this study employed the doctor blade method. Following the coating step, drying is carried out in two zones of a convective dryer. For the purposes of this study, the coating is not required to be fully dried after the drying phase. Instead, various conditions are simulated at the dryer's outlet by adjusting the drying parameters (temperature, heat and mass transfer coefficients). This approach allows for the emulation of sensor integration at any position along the dryer. Immediately downstream of the drying section is a measurement zone. Here, a dual-sided thickness measurement is performed using two chromatic confocal sensors (Precitec CHRocodile 2 DPS). The methodology and the operational principles of these sensors are elaborated in the subsequent section. Concurrently, a scattered light sensor (Optosurf OS500), detailed in vol. 1 [3], is employed to enhance data acquisition. Following the measurement section, a designated area facilitates the determination of area weight and porosity by cutting out samples using a precision template, followed by gravimetric analysis (Table 1).

2.2 Slurry preparation

The mixing procedure applied in this study was identical to that described in our previous publication (Vol. 1) [3]. The preparation of the slurry was carried out using a dissolver (Dispermat CN10, VMA Getzmann, Germany). Initially, graphite and carbon black were mixed in a dry blending step for 10 min at 300 rpm. Subsequently, the dry mixture was combined in three steps with a 2 % solution of sodium carboxymethyl cellulose (CMC). This was followed by mixing the blend for 45 min at 1500 rpm under simultaneous degassing and cooling. Afterward,

Table 1 Dry composition of the anode slurry used in this study

Component	Concentration (dry wt. -%)
Hitachi SMG-A (Graphite)	93
Timcal SuperC65 (Conductive carbon black)	1.4
Carboxy-Methyl-Cellulose "CMC" (Binder, Sunrose MAC500LC, Nippon Paper Industries)	1.87
Styrene–Butadiene Rubber "SBR" (Binder, Zeon Europe GmbH)	3.73

styrene–butadiene rubber (SBR) was added and stirred for an additional 10 min at 500 rpm. The final slurry had a solid content of 43 % and consisted of 57 % demineralized water.

2.3 Determination of the porosity

In general, the porosity ϵ of a porous layer is defined as the ratio of the void volume V_{void} to the total volume V_{total} of the layer:

$$\epsilon = \frac{V_{void}}{V_{total}}. \tag{1}$$

In the production of battery electrodes, porosity is typically considered only in the fully dried state. In this case, the porosity of the electrode $\epsilon_{electrode}$ can be directly determined from the area weight $m_{electrode}$, the density of the dry material ρ_{dry}, and the thickness of the dry electrode layer h_{dry}: [9]

$$\epsilon_{electrode} = 1 - \frac{m_{electrode}}{\rho_{dry} \cdot h_{dry}}. \tag{2}$$

The density of the dry material ρ_{dry} can be determined from the mass fractions x and the densities ρ of the individual components. For the anodes used, this yields:

$$\rho_{dry} = \frac{1}{\frac{x_{graphite}}{\rho_{graphite}} + \frac{x_{CMC}}{\rho_{CMC}} + \frac{x_{SBR}}{\rho_{SBR}} + \frac{x_{CB}}{\rho_{CB}}}. \tag{3}$$

The study on hand aims to investigate the development of porosity during the drying process, focusing on states where the electrode is not fully dry. In this case, the total volume V_{total} consists of the volume of the dry material V_{dry}, the void volume V_{void}, and the volume of the solvent $V_{solvent}$. By expressing the volumes of the dry material and solvent as the quotient of their respective masses M_{dry}, $M_{solvent}$ and densities ρ_{dry}, $\rho_{solvent}$, the porosity ϵ_{calc} for a specimen with a reference area A_{ref} can be determined at any time as:

$$\epsilon_{calc} = \frac{V_{void}}{V_{total}} = \frac{V_{total} - V_{dry} - V_{solvent}}{V_{total}} = \frac{A_{ref} \cdot h_{film} - \frac{M_{dry}}{\rho_{dry}} - \frac{M_{solvent}}{\rho_{solvent}}}{A_{ref} \cdot h_{film}} \tag{4}$$

To determine the porosity during drying, the drying process is interrupted, and the following procedure is conducted: Initially, the chromatic confocal sensors are employed for an in-line measurement of the film thickness h_{film}, as outlined in Sect. 3.1. A specimen with a reference area A_{ref} is cut out using a precision template, as described in Sect. 2.1. The total mass M_{total} is determined gravimetrically, which consists of the dry mass M_{dry} and the solvent mass $M_{solvent}$. Subsequently, the sample is fully dried in an oven, and the dry mass M_{dry} is determined gravimetrically. Finally, the solvent mass $M_{solvent}$ present at the time of measurement is calculated as $M_{solvent} = M_{total} - M_{dry}$.

3 Confocal chromatic measurements

The confocal chromatic measurement method is widely utilized in industrial manufacturing for reliable quality assurance. Figure 2 illustrates the operating principle of a chromatic confocal sensor. A polychromatic light beam is dispersed into its spectral components by a special optical system, with each wavelength focused at a different point along the optical axis. When the light interacts with a layer, it is reflected at the interfaces. The reflected light is spectrally analyzed by the sensor enabling precise determination of the distance to the reflective surface. Additionally, by analyzing the intensity of the reflected light, valuable insights can be gained about the reflectivity of the measured surface. The measurement principle even enables the evaluation of layer thickness in multiple stacked layers as long as they have sufficient transparency. However, this is not feasible for battery electrodes due to their high optical absorption. Despite this limitation, the chromatic confocal measurement method is widely recognized for its precision and ease of use in measuring layer thicknesses [10, 11].

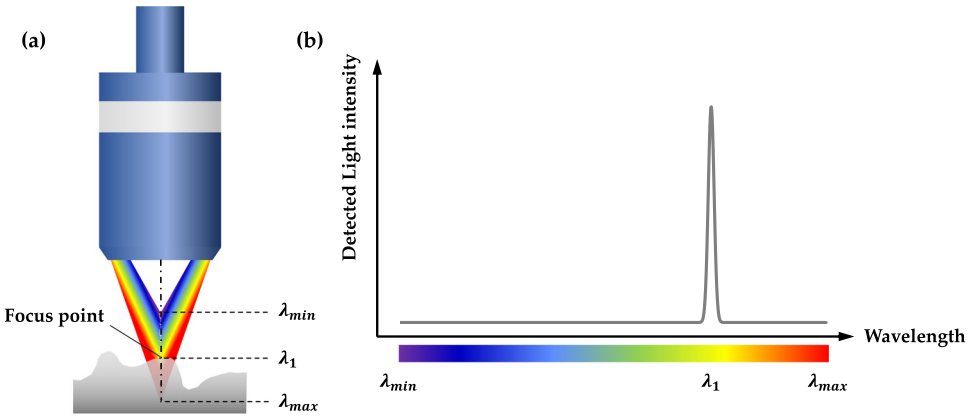

Fig. 2 Schematic representation of the principle of chromatic confocal thickness measurements: **a** the sensor generates polychromatic light, which is focused at different distances along the optical axis depending on its wavelength. Only light within a very narrow wavelength range is focused onto the surface to be measured. Analyzing the spectrum of the reflected light produces the signal indicated in (**b**), enabling precise determination of the distance to the measurement surface [12].

3.1 Double sided confocal chromatic measurements

A significant challenge in performing in-line measurements with chromatic confocal sensors arises from the vibrations of a moving measurement substrate. In the case of battery electrodes, the motion of the substrate belt complicates the accurate determination of layer thickness. To mitigate this issue, a dual-sided measurement configuration is employed, utilizing two precisely aligned sensors positioned above and below the substrate belt. To ensure a precise alignment of the sensors, the substrate between them is first removed. Subsequently, the fine adjustment of the sensor heads is carried out using precision screws until the signal from one sensor is accurately detected by the opposing sensor head. Since the signal is both emitted and detected in a centered manner, this configuration guarantees an optimal alignment of the sensor heads. Figure 3(a) illustrates the setup for dual-sided measurements and (b) the measurement signals recorded by both sensors. By summing the signals from the two sensors, the layer thickness can be determined with high accuracy. Analysis of the measurement signals indicates that the distance between the substrate web and the sensor heads fluctuates by up to 30 µm. Nevertheless, the summation of the sensor signals enables layer thickness determination with an accuracy of less than 1 µm, demonstrating the robustness of the dual-sided measurement approach. For the precise determination of layer thickness, a calibration with a known reference thickness is performed. During the experiments, a straightforward method for continuously verifying the measurement accuracy of layer thickness determination was to measure the uncoated substrate layer, which is known to have a thickness of 10 µm. A key parameter is not only the layer thickness itself but also the distribution of the calculated layer thickness signal, which provides a basis for characterizing the measurement surface, as illustrated in the bottom graph of Fig. 3c. Note, that the indicated interval $\pm 3\sigma$ corresponds to a total range of 6σ, as this representation facilitates clearer visualization in the figure. In the further part of the study, the 3σ interval is consistently used to characterize the layer surface.

3.2 Determination of surface roughness

In vol. 1 of the study, extensive focus was placed on the development of surface roughness during electrode drying [3]. This raises the question of how the measurement signals from the dual-sided chromatic confocal sensors evolve throughout the drying process. Figure 4 compares a wet electrode layer with a fully dried one. It is evident that the variability of the signal increases significantly from the wet film to dry film, rising from $3\sigma = 2.8$ µm to $3\sigma = 23.6$ µm. This can clearly be attributed to the increase in surface roughness, which was already demonstrated in vol. 1 using scattered light sensor measurements. The feasibility of characterizing surface roughness via chromatic confocal sensing was already established by Fu et al. [13]. These findings give rise to two central research questions:

1. Detection of Pore Emptying: Can chromatic confocal measurements detect the onset of pore-emptying with a precision comparable to that of scattered light sensors?
2. Insights into Pore Networks: Can the depth-resolved information obtained from the measurement signal be leveraged to infer the structural properties of the emerging pore network? Specifically, can parameters such as pore size or pore size distribution be quantitatively determined?

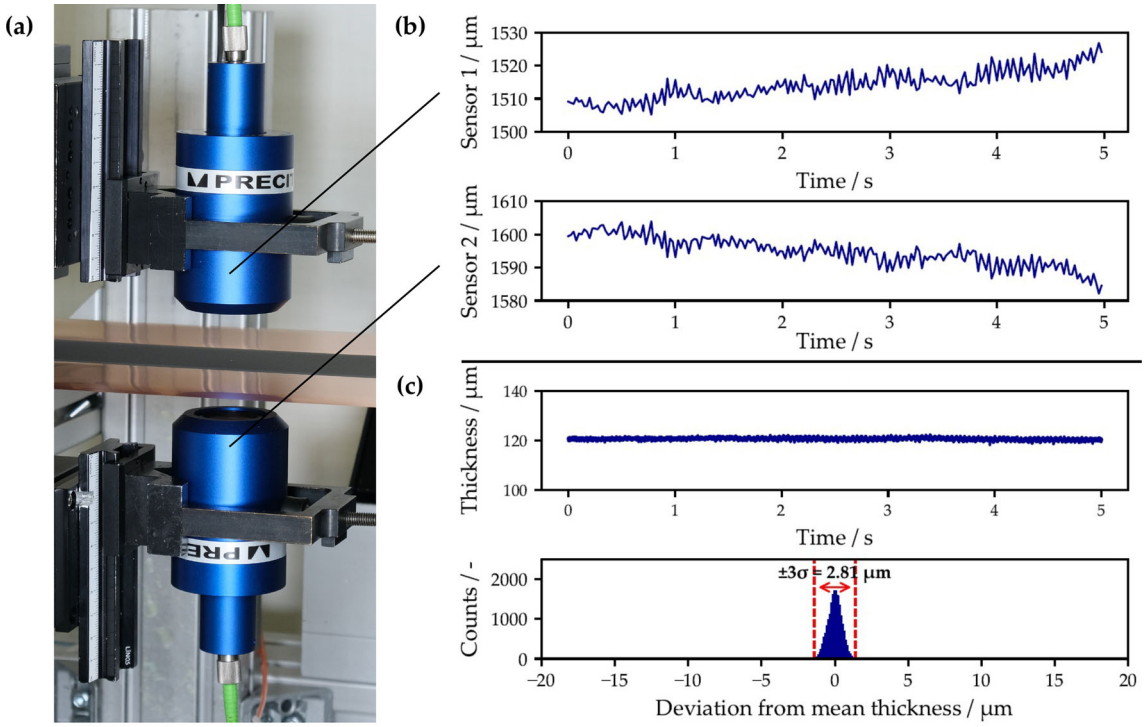

Fig. 3 Illustration of the double-sided measurement principle: **a** Two chromatic confocal point sensors precisely aligned and positioned above and below the substrate band. **b** Distance signals from both sensors recorded over a 5-second interval. **c** The sum of both signals resulting in the layer thickness signal, accompanied by the corresponding distribution of measurement values

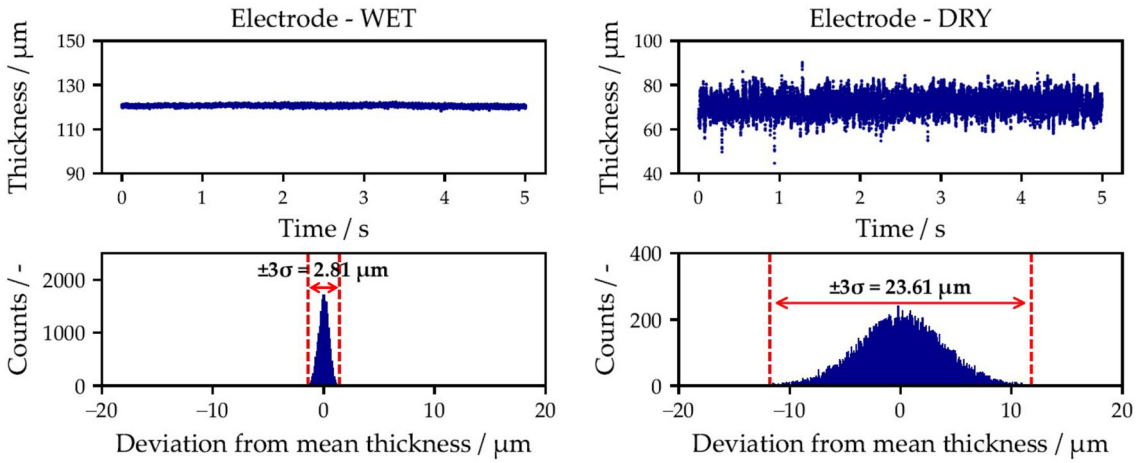

Fig. 4 Comparison of the thickness signal for a wet electrode (left) at the beginning of the drying process and a dry electrode (right) at the end of the drying process. The upper graphs display the determined layer thicknesses, while the lower diagrams illustrate the distribution of the thickness signal

4 Results and discussion

4.1 Evaluation of pore-emptying onset

To investigate whether chromatic confocal sensors can detect the onset of pore-emptying with a reliability comparable to that of scattered light sensors, the measurement signals of both sensor types were systematically compared during a controlled drying experiment. The experimental setup, as detailed in Sect. 2.1, positioned the scattered light sensor and chromatic confocal sensors in close proximity to ensure direct comparability. The results are

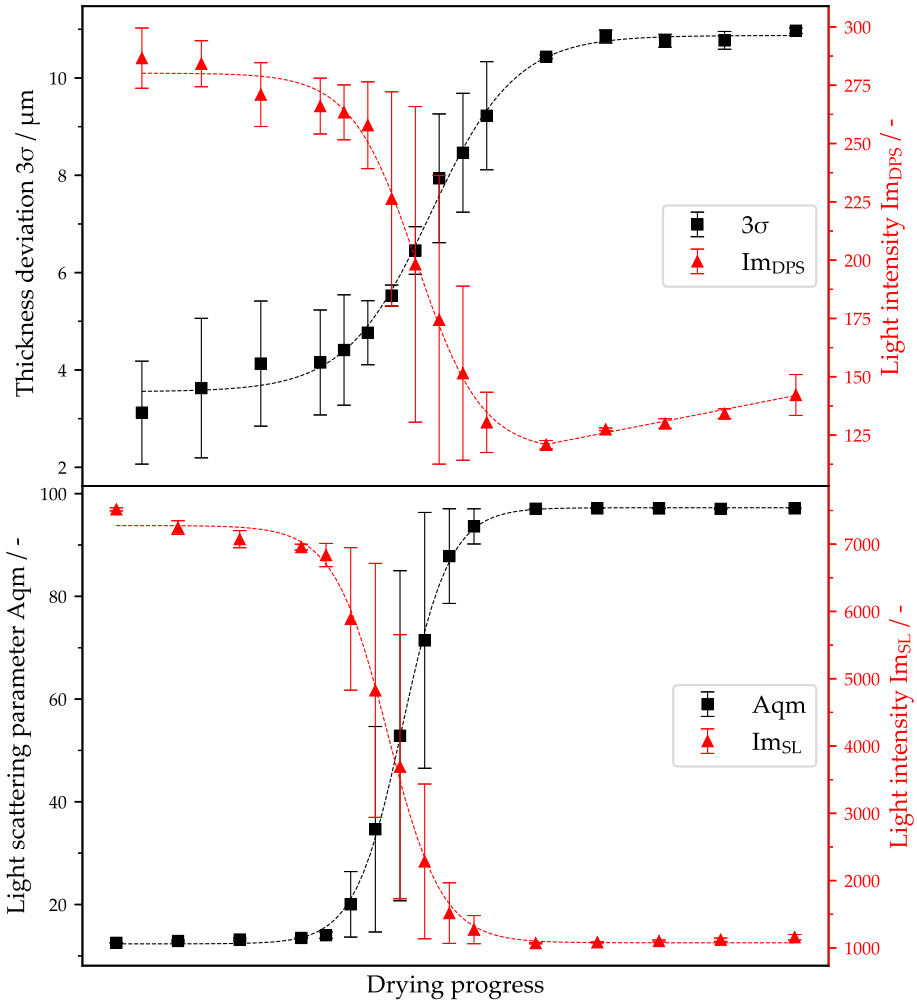

Fig. 5 Comparison of sensor signals during electrode drying: **a** Chromatic confocal sensors (DPS), Thickness deviation 3σ, Reflected light intensity Im_{DPS}; **b** Scattered light sensor (SL), Scattered light parameter Aqm, Reflected light intensity Im_{SL}; Test conditions: Initial area weight $m = 144\ g/m^2$, number of replicates per data point $n = 3$

presented in Fig. 5. The measurement data were fitted using logistic curves to illustrate their progression. Since the positions of the sensors in the experimental setup were fixed, the dryer settings (drying temperature and heat transfer coefficients) were adjusted in each trial to gradually increase the drying rates. Consequently, each data point originates from one individual experiment. Because the drying rates could not be quantified for all operating condition, the "drying progress" is plotted on the horizontal axis without scaling. Note that similar curve patterns emerge when measurement data are continuously recorded during a single experiment and plotted against drying time. This assumption is supported by the results presented in vol. 1 of the study [3].

The upper graph presents the data from the chromatic confocal sensors, while the lower graph shows the corresponding measurements from the scattered light sensor. In both graphs, the red curve represents the intensity of reflected light captured by the sensors, serving as an indicator of the electrode surface reflectivity. The black curve in the upper graph corresponds to the threefold standard deviation (3σ), as introduced in the previous section, which provides a measure of surface roughness. Similarly, the black curve in the lower graph represents the parameter Aqm, which characterizes light scattering and also indicates the surface roughness. A detailed description of the scattered light sensor, its operating principle, and the parameters Aqm and Im_{SL} is provided in vol. 1 of the publication [3].

The two sensors yield two distinct but comparable parameters, enabling a direct comparison of their performance. The resulting data demonstrate strong agreement between the two sensors, aligning with previously reported trends for the scattered light sensor. During the initial drying phase, prior to pore-emptying, the reflected light intensity for both sensors remains at a stable, high plateau, while 3σ and Aqm remain low and stable. As pore emptying commences, a transition phase begins, characterized by a steep increase in 3σ and Aqm, which eventually stabilizes at significantly higher levels. Simultaneously, the light intensity for both sensors decreases, reaching a minimum value. However, while the scattered light sensor's intensity value remains at a consistently low plateau, the intensity measured by the chromatic confocal sensors first increases after reaching its minimum, eventually stabilizing at its final value when the film is completely dry. The reason for this secondary increase in intensity is not entirely clear.

One plausible explanation is that residual solvent vapor in the air layer above the drying film influences the sensor's light detection through extinction and scattering effects, reducing the measured intensity. As drying progresses and solvent concentration in the air diminishes, the intensity measurement becomes predominantly determined by the surface characteristics of the electrode. This hypothesis is further supported by additional experiments in which convective airflow was introduced over the film during the late drying phase. This intervention caused an immediate increase in the intensity measured by the chromatic confocal sensors to its final stable value, providing strong evidence in favor of the proposed mechanism. It is further observed that the initial slope of the curves for the chromatic confocal sensor is slightly shallower compared to that of the scattered light sensor. Even in the very early stages of drying, a slight increase in the variable 3σ can be detected, and the Im curve for the chromatic confocal sensor also exhibits a flatter progression. Moreover, the error bars for the chromatic confocal sensors are significantly larger, particularly during the first half of the drying process, compared to those of the scattered light sensor. Nevertheless, the overall characteristic trends of the curves are identical for both sensor types. In Vol. 1 of the study, it was demonstrated through extensive transition experiments for the scattered light sensor that the increase in the roughness parameter Aqm corresponds precisely to the point at which drying rates must be reduced in a multi-stage drying process to avoid compromising the electrode quality. Given that the comparison of the sensors reveals the expected identical qualitative curve progression, this capability can be considered equally demonstrated for the chromatic confocal sensor.

4.2 Porosity determination

In the next step, the initial question will be addressed: whether depth-resolved information extracted from the measurement signal can be utilized to deduce the structural properties of the emerging pore network, with particular emphasis on porosity and pore sizes. For this purpose, multiple drying experiments were conducted again. The experimental setup described in Sect. 2.1 was employed once again, however without applying the scattered light sensor. Furthermore, the gravimetric method detailed in Sect. 2.3 was utilized to determine the area weight and porosity of the electrode. The results are presented in Fig. 6. The lower graph displays the sensor parameters 3σ and Im_{DPS} throughout the drying process. The qualitative trends of these curves are consistent with the measurements used for sensor comparison in the previous section. Insights are gained by correlating the trends of the sensor parameters with the quantities depicted in the upper graph, which illustrates the evolution of the electrode area weight m, the film thickness h_{film}, and the calculated porosity ϵ_{calc}. The film thickness was obtained from the measurements by the chromatic confocal sensors, while the area weight was determined following the

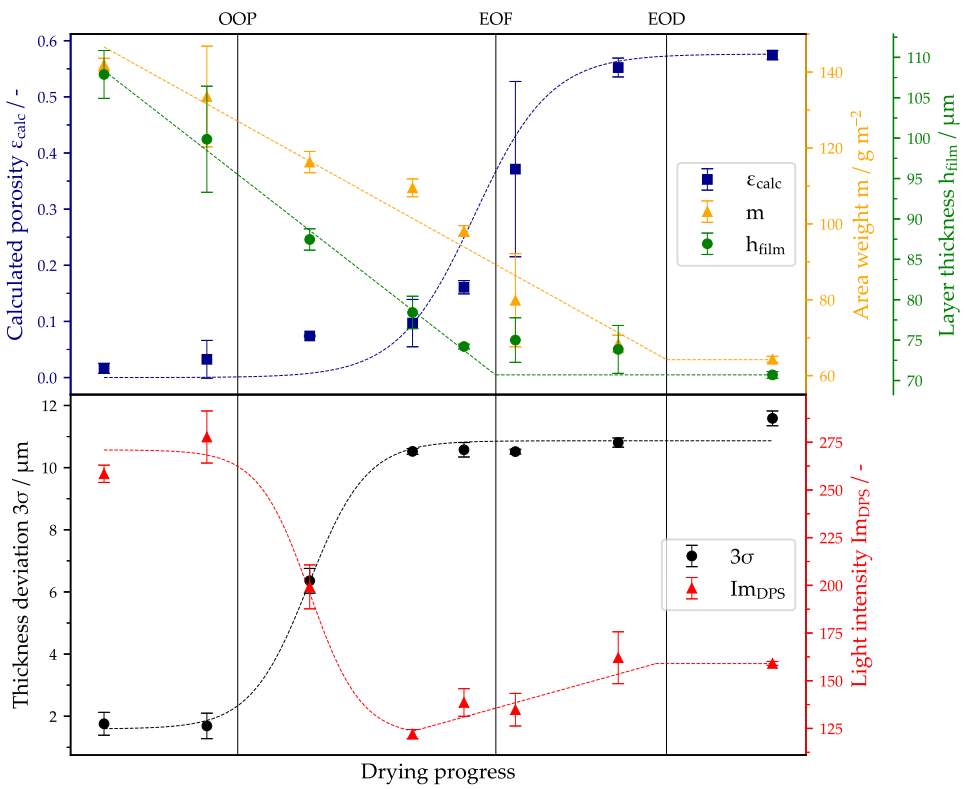

Fig. 6 Simultaneous measurement of film height h_{film}, areal weight m, and porosity ϵ_{calc} (top diagram), along with comparison to the variables measured by the chromatic confocal sensors 3σ and Im_{DPS} (bottom diagram). Characteristic points indicated: OOP: Onset of pore-emptying, EOF: End of film shrinkage, EOD: End of drying. Test conditions: Initial area weight $m = 141\ g/m^2$, number of replicates per data point $n = 3$

methodology described in Sect. 2.3. The porosity ϵ_{calc} was then calculated using Eq. 4, based on the area weight and film thickness.

From the measured data, various characteristic points during the drying process can be identified, which are indicated in the diagram. The onset of pore-emptying (OOP) was determined applying the method introduced by Jaiser et al. [6] to the 3σ curve, where the intersection of the tangent at the inflection point of the curve with the asymptote of the lower plateau is identified. Furthermore, the point marking the end of film shrinkage is denoted as EOF, a notation introduced by Kumberg et al. [14]. Therefore, a linear decrease in the layer height h was assumed. The theoretical EOF point is reached when the linear trend line of the layer height converges to its final value. Finally, the point marking the "end of drying" is labeled as EOD. Assuming a drying process entirely controlled by gas-phase diffusion, a linear trend line for the mass signal can be derived. When the trend line reaches its final value, the film can be considered completely dry. From this point onward, all signals remain constant. The onset of pore-emptying occurring well before the end of film shrinkage was already documented by Kumberg et al. [15]. In 2023, Janning [16] found that the breakthrough of pores at the bottom of the layer coincides temporally with the end of film shrinkage. These findings align well with the results of the present measurements. The simultaneous measurement of layer height and area weight, combined with the determination of porosity, provides valuable insights into the mechanisms dominating the different phases of pore structure emptying. By definition, porosity has an initial value of zero at the onset of drying, remaining so until the pore-emptying phase begins. As pore-emptying starts, porosity shows a gradual increase. During this phase, however, the evaporation of the solvent is largely compensated by the mechanism of film shrinkage. As film shrinkage approaches completion, the porosity begins to increase more steeply. From the end of film shrinkage onward, all evaporating solvent originates from the unloading of pores, leading to a continuous rise in porosity until it reaches its maximum value at the final stages of drying. Although the results provide valuable insights into the processes and mechanisms occurring during electrode drying, it becomes evident that the parameters derived from the chromatic confocal sensors, specifically 3σ and Im_{DPS}, are largely unable to detect events other than the onset of pore-emptying. After the transition region in the sensor signals, these parameters enter a saturation phase. The subsequent gradual increase in the Im_{DPS} signal is likely attributable to effects occurring in the gas phase and appears to be significantly influenced by airflow dynamics within the dryer. Consequently, this signal is not suitable for establishing correlations, such as tracking the progression of pore-emptying. Nevertheless, sensor measurements remain valuable for monitoring also later stages of the drying process, particularly for detecting the progression of film shrinkage.

5 Conclusion

The results of the initial experiments provide strong evidence that the electrode surface can be characterized just as reliably using chromatic confocal sensors as with the scattered light sensor investigated in Vol. 1 of the study. The signal profiles of both sensors show excellent qualitative agreement. The detection of the onset of pore-emptying, which is highly beneficial for implementing a three-stage drying process, should therefore be easily achievable with the chromatic confocal sensors. The authors suggest that the increase in detected light intensity Im_{DPS} observed near the end of drying should not be given excessive importance, as it is likely attributable to gas-phase effects.

Further, the drying process was investigated in greater detail using the chromatic confocal sensors. By combining layer thickness measurements by the sensors with determination of area weight and porosity during the drying process, valuable insights into the drying mechanisms were obtained. However, characterizing the drying state beyond the onset of pore-emptying using the parameters 3σ and Im_{DPS} does not appear to be feasible. Nonetheless, the chromatic confocal sensor remains a valuable tool for determining the final porosity at the end of the drying process.

In industrial electrode production, the initial wet film thickness after coating is typically measured, and the slurry composition is strictly controlled, ensuring that the area weight of the dry material is known. Consequently, measuring the final layer thickness enables a straightforward determination of the final porosity using Eq. 2. For this reason, searching for potential correlations between the final porosity and the standard deviation of the layer thickness signal 3σ at the end of drying does not seem practical. However, it might be possible to use the sensor signals to achieve a determination of the pore size distribution. This could be verified by analyzing the distribution of layer thickness signals in greater detail and align the results with the distribution of the pore sizes. Such a quantitative determination of a pore size distribution is, however, highly complex and requires advanced experimental techniques, such as mercury porosimetry, which were beyond the scope of this study. With regard to practical applications inside a dryer, chromatic confocal sensors offer several advantages. First, the sensors provide a measurement of the layer thickness, which alone represents a valuable parameter for determining the progress of drying. Additionally, the surface of the layer can be characterized using the parameters 3σ and Im_{DPS}, enabling the detection of the onset of pore-emptying. The sensor head and the processing unit are spatially separated, with the light signal captured by the sensor head being transmitted to the processing unit via an optical fiber. This design results in a very compact sensor head, facilitating easier integration within the interior of a technical dryer.

Furthermore, since the sensor head contains no electronics, it is highly robust to elevated temperatures and may be installed inside a dryer hood without requiring thermal insulation.

Acknowledgements The authors would like to acknowledge financial support from the Federal Ministry of Education and Research (BMBF) through the AQua cluster project "IQ-El" (Grant number: FKZ 3XP0359A). This work contributes to the research performed at the Center for Electrochemical Energy Storage Ulm-Karlsruhe (CELEST). The authors express their sincere gratitude to Precitec for their invaluable support. We deeply appreciate the fruitful collaboration, their assistance in resolving technical challenges, and the excellent partnership throughout this project.

Funding Open Access funding enabled and organized by Projekt DEAL.

Availability of data and materials The data that support the findings of this study are available from the corresponding author upon reasonable request.

Declarations

Conflict of interest The authors declare no conflict of interest.

Generative AI and AI-assisted Technologies in the writing process During the preparation of this work, the authors used generative AI technologies (DeepL/ChatGPT (...)) to improve readability and clarity. The authors reviewed and edited the content after usage and take full responsibility for the content of the publication.

References

1. M.M. Cerrillo-Gonzalez, M. Villen-Guzman, C. Vereda-Alonso, J.M. Rodriguez-Maroto, J.M. Paz-Garcia, Towards sustainable lithium-ion battery recycling: advancements in circular hydrometallurgy. Processes **12**(7), 1485 (2024)
2. G.V. Silva, M. Thomitzek, T. Abraham, C. Herrmann, T. Braunschweig, Simulation-based assessment of energy demand and costs associated with production scrap in the battery production. Simul. Produktion Logistik **2021**, 103–112 (2021)
3. J. Mohacsi, K. Ly, M. Birg, P. Scharfer, W. Schabel, In-line monitoring of a multi-stage drying process for battery electrodes: Vol. 1 - applying methods of scattered light measurement. Eur. Phys. J. Special Topics 1–9 (2024)
4. J. Kumberg, M. Müller, R. Diehm, S. Spiegel, C. Wachsmann, W. Bauer, P. Scharfer, W. Schabel, Drying of lithium-ion battery anodes for use in high-energy cells: influence of electrode thickness on drying time, adhesion, and crack formation. Energ. Technol. **7**(11), 1900722 (2019)
5. S. Jaiser, M. Müller, M. Baunach, W. Bauer, P. Scharfer, W. Schabel, Investigation of film solidification and binder migration during drying of li-ion battery anodes. J. Power Sources **318**, 210–219 (2016)
6. S. Jaiser, A. Friske, M. Baunach, P. Scharfer, W. Schabel, Development of a three-stage drying profile based on characteristic drying stages for lithium-ion battery anodes. Drying Technol. **35**(10), 1266–1275 (2017)
7. A. Altvater, J. Klemens, J. Borho, A. Smith, T. Heckmann, P. Scharfer, W. Schabel, Application of multistage drying profiles for accelerated production of li-ion battery anodes using infrared radiation: validation with electrochemical performance and structural properties. Energy Technol. 2301272 (2024)
8. M. Baunach, S. Jaiser, S. Schmelzle, H. Nirschl, P. Scharfer, W. Schabel, Delamination behavior of lithium-ion battery anodes: influence of drying temperature during electrode processing. Drying Technol. **34**(4), 462–473 (2016)
9. J. Klemens, L. Schneider, E.C. Herbst, N. Bohn, M. Müller, W. Bauer, P. Scharfer, W. Schabel, Drying of ncm cathode electrodes with porous, nanostructured particles versus compact solid particles: comparative study of binder migration as a function of drying conditions. Energ. Technol. **10**(4), 2100985 (2022)
10. M. Hillenbrand, B. Mitschunas, C. Wenzel, A. Grewe, X. Ma, P. Feßer, M. Bichra, S. Sinzinger, Hybrid hyperchromats for chromatic confocal sensor systems. Adv. Optic. Technol. **1**(3), 187–194 (2012)
11. J. Li, R. Ma, J. Bai, High-precision chromatic confocal technologies: a review. Micromachines **15**(10), 1224 (2024)
12. GmbH. Precitec and KG Co. Optical Sensor CHRocodile 2 DPS - Non-Contact Measurement for Layer Thickness: User Manual. Precitec GmbH and Co. KG (2020)
13. S. Fu, W.S. Kor, F. Cheng, L.K. Seah, In-situ measurement of surface roughness using chromatic confocal sensor. Procedia CIRP **94**, 780–784 (2020). (**11th CIRP Conference on Photonic Technologies**)

14. J. Kumberg, M. Baunach, J.C. Eser, A. Altvater, P. Scharfer, W. Schabel, Investigation of drying curves of lithium-ion battery electrodes with a new gravimetrical double-side batch dryer concept including setup characterization and model simulations. Energ. Technol. **9**(2), 2000889 (2021)
15. J. Kumberg, M. Baunach, J.C. Eser, A. Altvater, P. Scharfer, W. Schabel, Influence of layer thickness on the drying of lithium-ion battery electrodes-simulation and experimental validation. Energ. Technol. **9**(5), 2100013 (2021)
16. L. Janning, Investigation of microstructure formation and pore emptying in relation to slurry properties and drying conditions ("untersuchung der mikrostrukturausbildung und der porenentleerung in abhängigkeit von slurry-eigenschaften und trocknungsbedingungen"). Master's thesis, Karlsruhe Institute of Technology (Germany), Thin Film Technology (TFT) (2023)